THE JOURNAL OF PHYSICAL CHEMISTRY C

Article

Cite This: J. Phys. Chem. C 2019, 123, 4433−4440

pubs.acs.org/JPCC

Unraveling the Defect Emission and Exciton−Lattice Interaction in Bilayer WS_2

Qing-Hai Tan,[†,‡] Shu-Liang Ren,[†,‡] Tao Shen,[†,‡] Xue-Lu Liu,[†,‡] Wei Shi,[†] Yu-Jia Sun,[†,‡] Hui-Xiong Deng,[†,‡] Ping-Heng Tan,[†,‡,§] and Jun Zhang*[,†,‡,§,∥]

[†]State Key Laboratory of Superlattices and Microstructures, Institute of Semiconductors, Chinese Academy of Sciences, Beijing 100083, China

[‡]Center of Materials Science and Optoelectronics Engineering, University of Chinese Academy of Sciences, Beijing 100049, China

[§]CAS Center of Excellence in Topological Quantum Computation, University of Chinese Academy of Sciences, Beijing 101408, China

[∥]Beijing Academy of Quantum Information Science, Beijing 100193, China

Supporting Information

ABSTRACT: Defect states and exciton of two-dimensional semiconductors play an important role in fundamental research and device applications. Here, we reported the defect emissions and exciton−lattice interaction of bilayer WS_2. These defect emissions show a very narrow linewidth, doublet peaks, spatial localization, saturation with pumping power and can survive up to 180 K. The behavior of these defect emissions means it should be a good candidate as a single photon source. Besides defect emissions, direct exciton and two indirect excitons due to band-to-band transition are identified. By analyzing the temperature-dependent photoluminescence (PL) spectra of excitons, we obtained the Debye temperature, exciton−phonon coupling constant, and pressure coefficient terms of all excitons. Combining the PL experiments and density functional theory calculations, we attributed two indirect excitons to the Λ−*K* and Λ−Γ transitions, respectively. Our study not only gives a better understanding of the defect emissions and energy band structure in multilayer materials, but also provides an opportunity for defect and band engineering in two-dimensional layered systems.

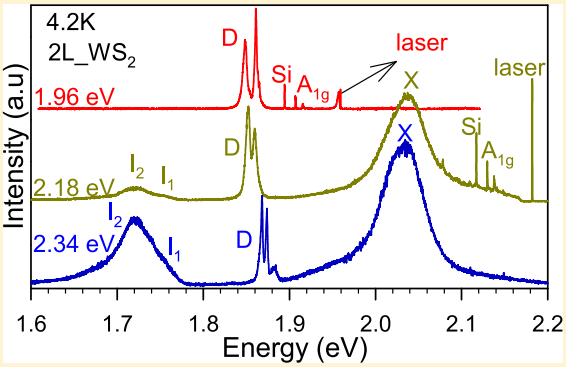

INTRODUCTION

The defect states buried in the band gap and exciton states due to band-to-band transition are very important for understanding the semiconductor optical properties and designing related optoelectronic devices. The defects, especially the single isolated defect in solids, have been investigated for applications in quantum control,[1,2] single photon sources,[3] etc. For example, the nitrogen (or Si) vacancies in diamonds have been used as a stable solid-state single photon source and quantum key distribution.[2−4] Remarkably, layered transition metal dichalcogenides (TMDs) provide a unique platform to study the defect-induced photoluminescence (PL) for its novel electronic and optical properties, such as the transition from the indirect to direct band gap with the thickness down from bulk to monolayer,[5,6] large exciton binding energy,[6,7] and valley polarization.[8,9] Among the TMDs family, single photon emission was first discovered in monolayer WSe_2 by several independent research groups,[10−13] which stimulated the search for single photon emission in other layered materials.[14,15] Up to now, the single photon emission from the defect has also been observed in layered GaSe,[16] hexagonal boron nitride (hBN),[17,18] and monolayer WS_2.[19,20] However, most of these reports about single photon emission in TMDs just focused on monolayer samples, whereas for the bilayer or more layers, few of them have been reported.[19,21] Note that although the single photon emission in hBN has been observed at room temperature,[15,18] for TMDs, the single photon emission just survived below 40 K so far, which limits its potential applications.

On the other hand, the indirect-to-direct transition in these TMD compound results from the local shift of the valence band minimum (VBM) and the conduction band maximum (CBM) in the Brillouin zone.[5,6,22,23] In the single layer, the CBM and VBM coincide at the *K* point, making them a direct gap semiconductor. In multilayers, the valence band hill at the Γ point is raised above the hill at the *K* point. Similarly, the conduction band valley at the Λ point (midpoint between *K* and Γ) shifts downward with the increasing interlayer interaction. In contrast, the states near the *K* point are comparatively less susceptible to the number of layers. In

Received: November 13, 2018
Revised: January 25, 2019
Published: January 25, 2019

DOI: 10.1021/acs.jpcc.8b11011
J. Phys. Chem. C 2019, 123, 4433−4440

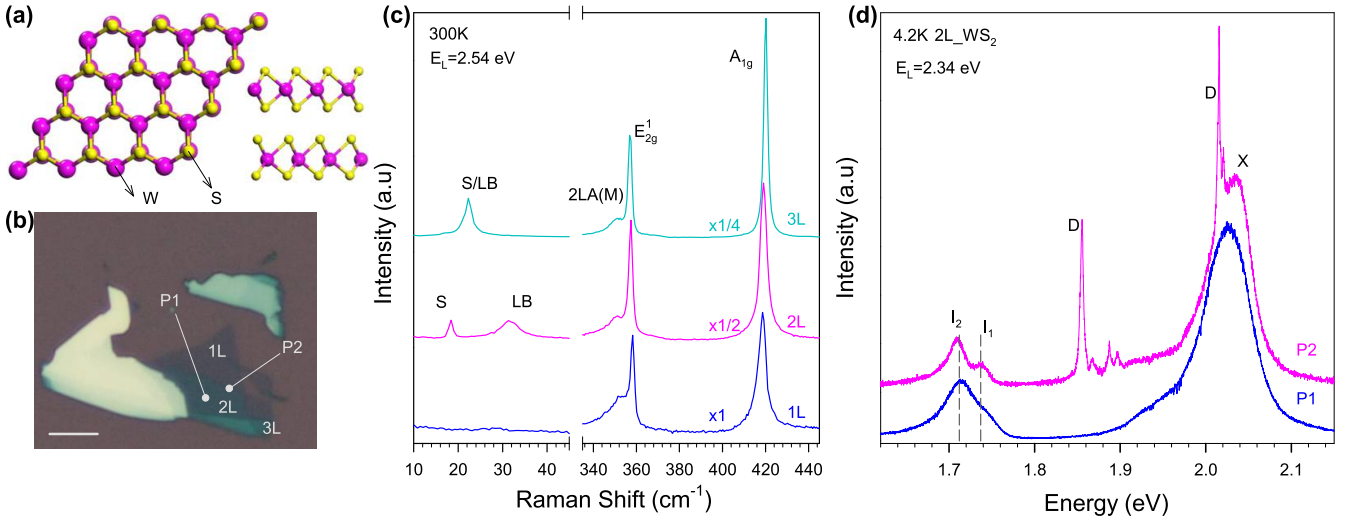

Figure 1. Raman and photoluminescence (PL) spectra of few-layer WS_2. (a) A schematic atomic structure of bilayer WS_2 from top and side view, respectively. (b) The optical image of the monolayer (1L), bilayer (2L), trilayer (3L) WS_2 samples, with scale-bar 5 μm. (c) The ultralow and high frequency Raman spectra of 1-3L WS_2 with 2.54 eV excitation (E_L) at room temperature. The S and LB represent the shear and layer breathing modes, respectively. (d) The PL spectra collected from the center (P_1) and edge (P_2) of 2L WS_2 with 2.34 eV excitation at 4.2 K. The I, D, and X represent the indirect exciton, defect, and direct exciton emissions, respectively.

multilayer TMDs, the optical transition from $K-K$, $K-\Gamma$, $\Lambda-K$, and $\Lambda-\Gamma$ corresponds to one direct exciton and three indirect excitons, respectively. By conducting the photon emission spectra, these extreme points of the conduction band and valance band can be identified. Zhao et al. have demonstrated that the indirect optical transition originates from $\Gamma-K$ in the Brillouin zone of MoS_2, $\Lambda-\Gamma$ in WS_2, whereas both $\Gamma-K$ and $\Lambda-\Gamma$ are observed in multilayer WSe_2[22] by using temperature-dependent PL spectra from 123 to 423 K. However, in this temperature range, the indirect excitons show one broad peak and it is not possible to resolve the $K-\Gamma$ and $\Lambda-\Gamma$ indirect transitions. Besides, the electron–phonon coupling of these excitons is also unknown. Therefore, further experiments with higher spectral resolution, lower temperature, and theoretical calculations are required to identify the indirect exciton transitions as well as their exciton–phonon coupling.[24]

Here, we studied the defect emissions and direct/indirect exciton transition in bilayer WS_2 from 4.2 K to room temperature. At low temperatures, we observed a series of sharp defect emissions at some edge positions of bilayer WS_2 samples, where these defect emission peaks can survive up to 180 K. The defect emissions show a saturated behavior with increasing pumping laser power. The above features hint that these defect emissions are good candidates for single photon sources. By using a resonant excitation, the PL background from direct and indirect excitons can be totally suppressed and one background-free sharp defect spectrum is obtained. Besides, two indirect exciton peaks I_1 and I_2 were clearly observed at low temperatures. Moreover, the indirect exciton I_2 shows a redshift, whereas I_1 show a blueshift with increasing temperature. Meanwhile, the intensity of these two indirect excitons shows a competitive behavior with the changing temperature. By comparing the experimental data with the density functional theory (DFT) calculations, we identified I_1 and I_2 as $\Lambda-K$ and $\Lambda-\Gamma$ transitions, respectively. The calculation results show that the band crossover will occur between different transition processes by applying the stress (or change temperature). By fitting the temperature dependence of exciton energy, the Debye temperature, exciton–phonon coupling constant, and pressure coefficient terms of direct and indirect excitons are obtained.

EXPERIMENTAL SECTION

The samples were prepared from bulk WS_2 crystals onto a 90 nm SiO_2/Si substrate by using the mechanical exfoliation technique. Raman and PL measurements on WS_2 samples were undertaken in backscattering geometry with a Jobin-Yvon HR800 system equipped with a liquid-nitrogen-cooled charge-coupled detector. The Raman measurements were undertaken with a 100× objective lens (NA = 0.9) and an 1800 lines mm^{-1} grating at room temperature, whereas a 50× long-working-distance objective lens (NA = 0.5) was used for temperature-dependent PL measurements. The excitation laser (E_L) line of 2.54 eV is from an Ar^+ laser, 1.96 eV line is from a He–Ne laser, 2.34 and 2.18 eV lines are from a Kr^+ laser. To avoid the heating effect on the samples, the laser power was kept below 0.3 mW. A Montana cryostat system was employed to cool the samples down to 4.2 K under a vacuum of 0.1 mTorr.

RESULTS AND DISCUSSION

The monolayer (1L) MX_2 is composed of an X–M–X (X = S, Se, Te, M = Mo, W) unit cell, where the M atoms are sandwiched between the two layers of X atoms. For a bilayer (2L) MX_2 with the 2H structure, the M atoms in the top layer vertically overlap with the X atoms in the bottom layer, as shown in Figure 1a. Therefore, the bilayer MX_2 has space-inversion symmetry and presents many different physical behaviors compared with the monolayer, such as the absence of valley polarization and second harmonic generation in 2L MX_2.[8,9,26] Figure 1b shows the optical image of few-layer WS_2 samples on the SiO_2/Si substrate with 90 nm SiO_2, where P_1 and P_2 are the center and edge positions of the 2L WS_2 samples, respectively. To identify the layer number of WS_2 samples, we first measured the Raman spectra (as shown in Figure 1c) and PL spectra (as shown in the Supporting Information Figure S1a) of 1-3L WS_2 at room temperature. In the ultralow frequency region (<50 cm^{-1}), no Raman modes

DOI: 10.1021/acs.jpcc.8b11011
J. Phys. Chem. C 2019, 123, 4433–4440

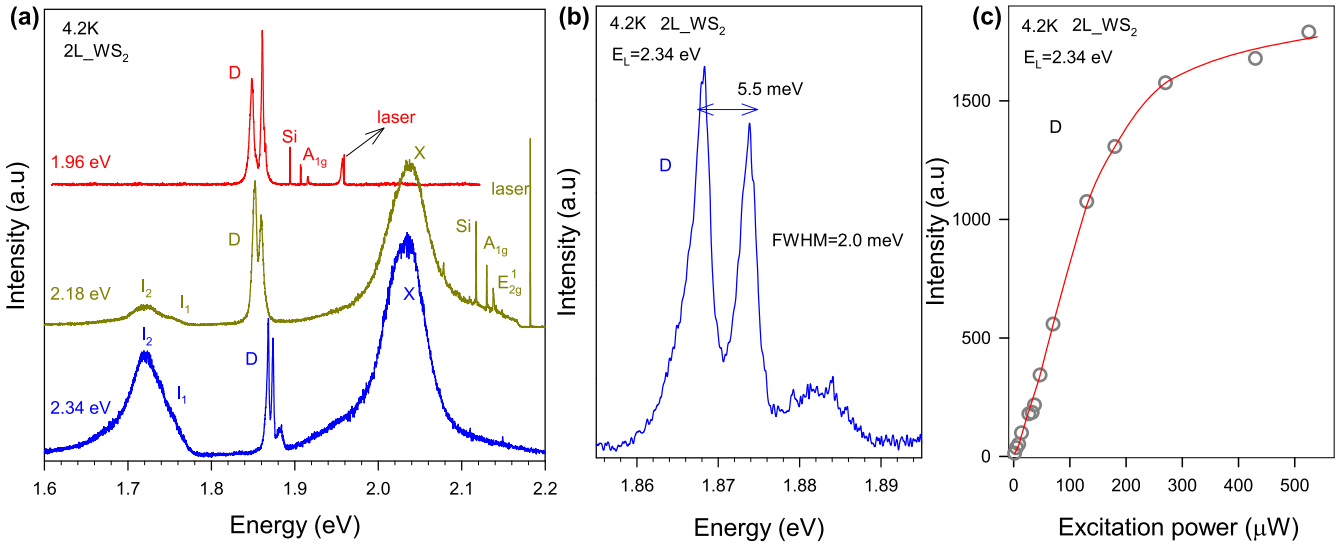

Figure 2. PL spectra of 2L WS_2 at 4.2 K. (a) The PL spectra with three different excitation laser lines. (b) The typical of defect emission with 2.34 eV excitation. (c) The power dependence of defect emission (the left one in b).

were observed in monolayer WS_2 owing to the lack of interlayer coupling,[27−29] whereas for 2L and 3L WS_2, one shear (S) mode and one layer breathing (LB) mode are observed with different frequencies, respectively. Since the frequencies of S and LB modes are strictly dependent on layer numbers,[28,30−32] we can use these modes to identify the layer numbers of WS_2. On the other hand, the indirect band gap of WS_2 is also layer-dependent,[23] which could serve as another characterization tool of layer numbers in WS_2, as shown in the Supporting Information Figure S1a. In the high frequency region, the E^1_{2g} modes show a redshift, whereas A_{1g} modes show a blueshift with increasing layer numbers. The shift of E^1_{2g} may result from the stacking induced structural changes or long-range Columbic interlayer interactions, whereas the shift of A_{1g} may result from out-of-phase displacement as layer numbers increase.[33−35] The frequency differences between E^1_{2g} and A_{1g} modes can also be used to identify the layer numbers of WS_2.[33,34] All of these results show that our samples are indeed 1-3L WS_2.

Then, we focus on the PL spectra of 2L WS_2. We measured the PL spectra of 2L WS_2 at different sample locations with 2.34 eV excitation at 4.2 K. One direct exciton at 2.03 eV and two indirect exciton peaks at 1.71 and 1.74 eV were clearly observed. Similar results were also observed in 3L WS_2 at 4.2 K, as shown in Figure S1b. Besides the direct and indirect exciton peaks, we also observed some narrow peaks at around 1.86 and 2.01 eV on the edge regime of 2L WS_2, as shown in Figure 1d. Two indirect exciton peaks are observed for all regions of 2L WS_2, whereas these narrow peaks are very sensitive to the sample location. According to the position-sensitive characteristic of these narrow peaks, we can speculate that these narrow peaks may originate from the exciton states bound to the isolated defects or crystal deformation potentials.[10−12,16] There are several possible origins for the isolated defect, for example, the S vacancy both in top and bottom layers of bilayer WS_2.[2525] However, the nature of the defects here is not clear now. Here, we simply mark them as D peaks.

To further study these D peaks, we used three lasers of 2.34, 2.18, and 1.96 eV to measure the PL spectra at 4.2 K at the same sample point, as shown in Figure 2a. It is obvious that the spectra are similar under 2.18 and 2.34 eV excitation, where the indirect excitons are composed of two peaks and D peaks are at around 1.86 eV. A small difference is that the relative intensity of direct and indirect exciton peaks is significantly changed under these two excitation wavelengths. When the excitation energy is lower than the direct band gap and close to the defect level at low temperatures, for example, 1.96 eV, all of the direct and indirect exciton peaks vanished, but the D peaks are more obvious. This is because the excitation energy of 1.96 eV is very close to the defect level. It is well-known that the resonant or near-resonant excitation can not only efficiently enhance the photon emission efficiency but also is basically important to study the coherence and dephasing mechanisms of few-level quantum systems, like in quantum dots.[36,37] Furthermore, under this near-resonant excitation conditions, we measured the PL spectra of defect emission of 2L WS_2 at different times, as shown in Figure S2. Obviously, most of these spectra show obvious doublet peaks but the relative intensity of doublet peaks is varied. One possible reason is that the measured sample point may not be exactly at the same position for each experiment. Besides, these defect emissions show a blinking phenomenon with time, which is usually due to the switching between dark and bright quantum state as reported on the defect emissions of monolayer WSe_2[11] and TMD heterostructures.[38,39] Therefore, the blinking effect may be another reason for the difference between these spectra excited by 1.96 eV.

We note that most of the D peaks here display a doublet structure with a narrow linewidth in all excitation energies at low temperatures. Because of the anisotropic electron−hole exchange interaction, the localized neutral exciton in a defect will split into two states and lead to the observation of doublet peaks, which is consistent with previous reports.[10−13] Figure 2b shows the D peaks in the range 1.855−1.895 eV with 2.34 eV excitation at 4.2 K. Two D peaks are located at around 1.874 and 1.868 eV, respectively. The energy difference between these doublet peaks is ~5.5 meV. The full width at half maximum of these two D peaks is about 2.0 meV. Such a narrow linewidth and doublet feature indicates that these D peaks in 2L WS_2 may belong to single photon emissions. Similar results have been observed in monolayers WSe_2 and

DOI: 10.1021/acs.jpcc.8b11011
J. Phys. Chem. C 2019, 123, 4433−4440

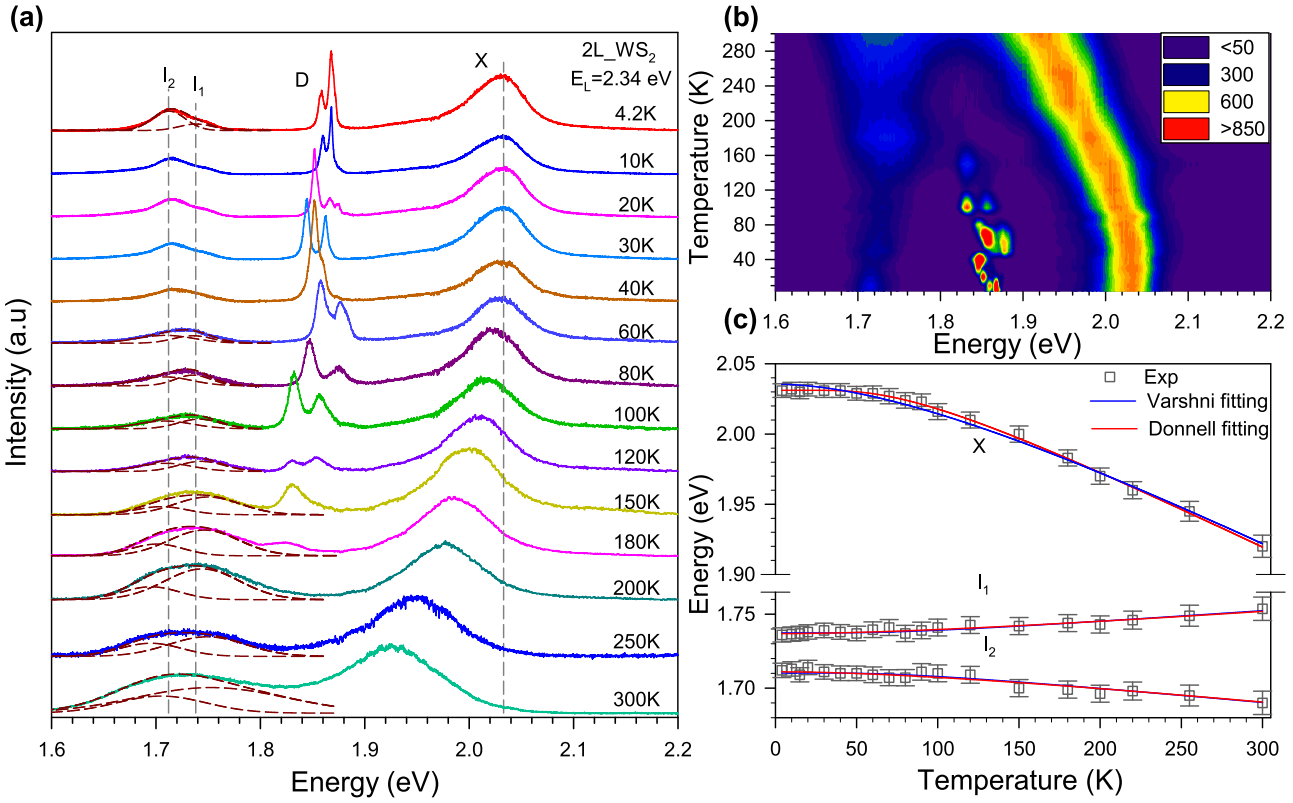

Figure 3. Temperature-dependent PL spectra of bilayer WS_2. (a) The evolution of indirect exciton, defect emission, and direct exciton transition with the increasing temperature. The dark red dashed lines are the fitting results of two indirect excitons I_1 and I_2, and the gray dashed lines are a guide to the eye. (b) The PL spectra of the two-dimensional (2D) pseudocolor plot of bilayer WS_2 from 4.2 to 300 K, here the intensities are normalized to the X (direct exciton) peaks. (c) The peak energies of direct exciton X and indirect exciton I_1 and I_2 as a function of temperature, the data are extracted from (a). The blue and red lines are the fitting results by Varshni and O'Donnell equation, respectively.

WS_2.[10−13] We also performed a power-dependent PL measurement, as shown in Figure 2c. As the excitation power increases, the intensity of the defect emissions first increases with laser power and then shows a saturation behavior above 300 μW. This saturation behavior can be described well by an atom-like two-level energy model. To check whether these defect emissions are single photon emission or not, we have tried to measure the second-order correlation function $(g^{(2)}(\tau))$ of these defect emissions. Unfortunately, owing to the weak intensity and blinking effect of the D emission in 2L WS_2, we failed to obtain the signal of second-order correlation function of these defect emissions, which are still waiting for further studies to confirm whether they are really single photon emission or not.

To further study the temperature-dependent evolutions of direct exciton, indirect exciton, and defect emissions, we measured the PL spectra of 2L WS_2 from 4.2 to 300 K. As shown in Figure 3a, with the increasing temperature, the intensity ratio between I_1 and I_2 gradually increases from below 0.5 at 4.2 K to over 1 at around 80 K. This indicates that the indirect excitons are dominated by I_2 at low temperature and then gradually replaced by I_1 with the increasing temperature. Interestingly, the defect emission in 2L WS_2 can survive up to 180 K, which is much higher than the highest emission temperature of defect states in monolayer WSe_2. Although the intensities of these defect emissions greatly decrease when the temperature exceeds 100 K, they can still be resolved. It means that these isolated defect emissions in multilayer WS_2 can work at a higher temperature. All of the linewidths of direct excitons, indirect excitons, and D peaks are broadened with the increasing temperature due to the thermal relaxation process.[40] The linewidths of D peaks are always much narrower than the direct/indirect exciton peaks. This is because the defect emissions are usually from exciton states bound to defect or the confinement potential formed by crystal deformations,[10−12,16] whereas the direct/indirect exciton peaks are from the transitions between different valleys at the conduction band to valence band hill in the Brillouin zone. Figure 3b shows the relative intensity change of indirect excitons and D peaks. Obviously, the relative intensity of indirect excitons increases with the increasing temperature. It means that the phonon-assisted indirect transitions gradually dominate the exciton transition process at higher temperatures due to more phonon population. Meanwhile, the intensity of the D peak is stronger at lower temperatures due to the much faster radiation recombination rate.

The peak energies of D peaks are weakly dependent on the temperature, but the indirect and direct exciton peaks show more obvious shift with the changing temperature as shown in Figure 3c. The electron−phonon interaction plays a key role in the photoelectric properties of semiconductors, for instance, the luminescence,[41,42] phonon[24,31,43] and intraband hot carries.[44] As the exciton moves through the crystal lattice, it interacted with phonons and then scattered by phonons. During the exciton scattering processes, phonon absorption is completely dominated at low temperatures because phonon population numbers are very small, but both phonon absorption or emission process contribute equally to the

DOI: 10.1021/acs.jpcc.8b11011
J. Phys. Chem. C 2019, 123, 4433−4440

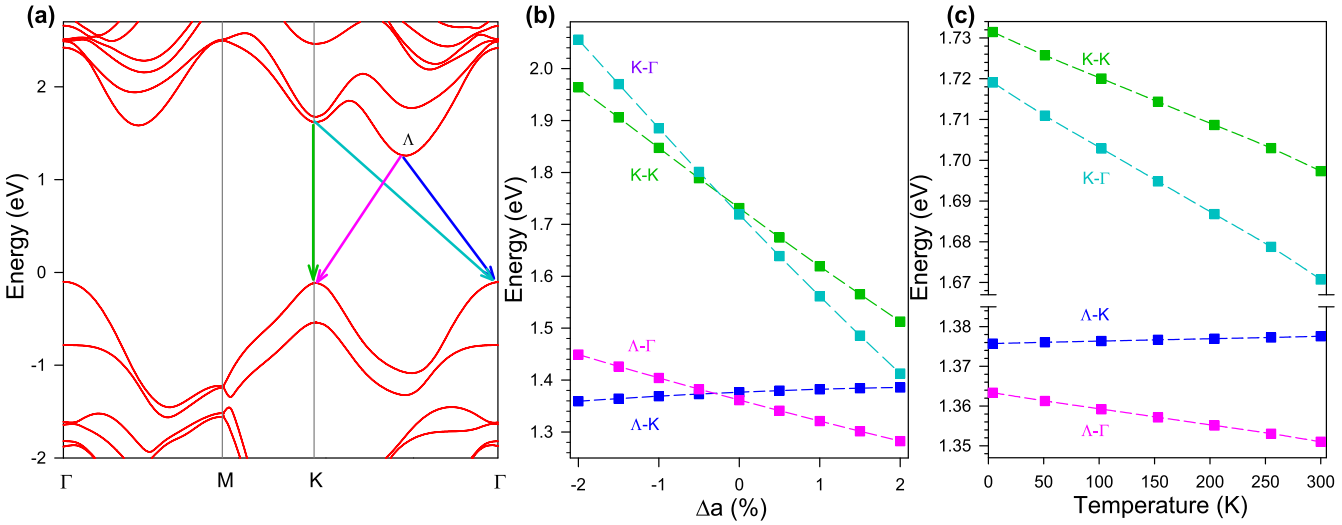

Figure 4. DFT calculation of the electronic band structure of bilayer WS_2. (a) The calculated energy band structures at 0 K. (b, c) The calculated evolution of direct and indirect transitions depending on the in-plane strain (b) and temperature (c).

exciton scattering as the temperature is of the order of the Debye temperature.[22,45] Therefore, the peak shifts of direct exciton with temperature are negligible when the temperature is below 80 K, and then it shows a linear decrease with increasing temperature of above 80 K, as shown in Figures 3a and S3a. Moreover, the direct exciton is much more sensitive to sample temperature than two indirect excitons, suggesting that the direct exciton has larger exciton−phonon coupling.

First, we used the Varshni equation to fit the experimental results, as shown by the blue curve in Figure 3c. The Varshni equation can be written as:[47] $E_g(T) = E_g(0) - \frac{\alpha T^2}{T+\beta}$, where $E_g(0)$ is the exciton energy at 0 K, α and β are fitting parameters characteristic of a given material, and α and β reflect temperature coefficient of the exciton shift and the Debye temperature of lattice, respectively. From the fitting parameters, we obtained the Debye temperature of bilayer WS_2 of around 200 K, which is consistent with previous reports.[46] The detailed fitting results can be found in Table S1 in the Supporting information. Because the electron−phonon coupling is not considered in the Varshni equation, the fitting curve for X peaks cannot match well with the experimental results, especially below 100 K. Then, we used the O'Donnell equation to fit the experimental results, as shown by the red curve in Figure 3c. The O'Donnell equation can be written as:[48] $E_g(T) = E_g(0) - S\langle\hbar\omega\rangle\left[\coth\frac{\hbar\omega}{2kT}\right]$, where S is the exciton−phonon coupling constant and $\langle\hbar\omega\rangle$ is the average phonon energy. Obviously, the fitting results match the experimental results of X peaks very well from 4.2 to 300 K, suggesting that the electron−phonon coupling is an indispensable part for the temperature-dependent shift of the direct exciton transition at low temperatures. The detailed fitting results can be found in Table S2 in the Supporting Information. On the basis of our fitting results, $\langle\hbar\omega\rangle \simeq 21$ meV for all of X, I_1, and I_2 data, implying that the average phonon energy is around 21 meV for all direct and indirect exciton transition processes, whereas S is equal to 3.33 ± 0.87, -0.45 ± 0.049, and 0.59 ± 0.04 for X, I_1, and I_2, respectively, implying that X has a larger electron−phonon coupling strength constant than two others. This is why the X exciton is more sensitive to temperature than I_1 and I_2 excitons.

From the thermal dynamic relationship,[49] $\left(\frac{\partial E}{\partial T}\right)_P = \left(\frac{\partial E}{\partial T}\right)_V - \frac{\beta}{\chi}\left(\frac{\partial E}{\partial P}\right)_T$, where the two terms $\left(\frac{\partial E}{\partial T}\right)_V$ and $\left(\frac{\partial E}{\partial P}\right)_T$ are corresponding to the temperature-induced energy shift caused by changes in the electron−lattice interaction and the lattice parameter (pressure efficiency), respectively, β and χ are the thermal expansion coefficient and isothermal compressibility, respectively. On the basis of this equation, we can obtain the lattice expansion term (pressure efficiency) $\left(\frac{\partial E}{\partial P}\right)_T$ of the exciton shift once we measured the temperature-dependent exciton shift term $\left(\frac{\partial E}{\partial T}\right)_P$ and vice versa, if we know the electron−lattice interaction term $\left(\frac{\partial E}{\partial T}\right)_V$. It is around 0.1 meV/K for the direct exciton based on previous reports.[49] Supposing the $\left(\frac{\partial E}{\partial T}\right)_V$ term is proportional to the exciton−phonon coupling constant S as we mentioned in O'Donnell fitting, we can obtain the $\left(\frac{\partial E}{\partial T}\right)_V$ term for two indirect excitons. In Figure S3, we plotted the calculated $\left(\frac{\partial E}{\partial P}\right)_T$ and measured $\left(\frac{\partial E}{\partial T}\right)_P$ for X, I_1, and I_2. We also listed our results and other reports in Table S3 in Supporting Information. The calculated $\left(\frac{\partial E}{\partial P}\right)_T$ term of direct exciton X at 100 K is around 9.64×10^{-3} and 7.37×10^{-3} meV/atm for the O'Donnell equation and Varshni equation fittings, respectively. These two calculated values are very close, implying that the energy shifts are dominated by the lattice thermal expansion for the temperature above 100 K. Meanwhile, these calculated results are consistent with the previous reported value (5.9×10^{-3} meV/atm).[49] Our results provide a convenient method to evaluate the temperature and pressure coefficients of 2D materials.

Besides, as shown in Figure 3c, the peak shifts of two indirect excitons show opposite temperature dependence, where I_1 is blueshifted but I_2 is redshifted with the increasing temperature. This phenomenon results from the highly anisotropic thermal expansion of the lattice and the corresponding evolution of the band structure, resulting in a

DOI: 10.1021/acs.jpcc.8b11011
J. Phys. Chem. C 2019, 123, 4433−4440

distinct peak shift for indirect transitions involving the K and Λ (midpoint along $\Gamma-K$) hill of the valance band. To give a clear understanding of the origin of two indirect excitons in bilayer WS_2, we used the density function theory (DFT) method to calculate its energy band structure at 0 K, as shown in Figure 4a. It has been well-established that for direct gap monolayer TMDs, the CBM and VBM coincide at the same K point;[5,6] whereas for the multilayer, there are two valleys at K and Λ (midpoint between K and Γ) points in the conduction band.[22,50] As shown in Figure 4b, we also plotted the electronic transition energies $K-K$, $K-\Gamma$, $\Lambda-K$, and $\Lambda-\Gamma$ as a function of in-plane lattice expansion for 2L WS_2. With the increasing in-plane lattice constant, the energy of transitions from $K-K$, $K-\Gamma$, and $\Lambda-\Gamma$ decrease, whereas $\Lambda-K$ transition energy increases. Since the energy difference between the Γ and K hill maximum is as small as 15 meV for bilayer WS_2 based on the DFT calculation results, we expect to observe two crossovers, that is, one is the band crossover between $\Lambda-K$ and $\Lambda-\Gamma$ indirect emission peaks due to the opposite strain dependence and the other one is between the $K-K$ direct exciton and $K-\Gamma$ indirect exciton due to different strain coefficients.

Next, we examined the effects of thermal expansion, which is a composite effect of in-plane and out-of-plane expansion explained above. According to the temperature-dependent ultralow frequency Raman spectroscopy, the shifts of S and LB modes are negligible.[31] It indicates that the interlayer interaction strength is unchanged and, thus, the interlayer distance is almost unchanged from 4.2 to 300 K. Moreover, for the same TMD materials, although the indirect band gaps are layer-dependent,[5,6,8,22,23] the interlayer interaction strength is constant from the bilayer to bulk samples. Meanwhile, the out-plane expansion mainly affects the indirect transition,[22] but the energy shifts of indirect excitons are small in our temperature-dependent PL experiment. Therefore, it is reasonable to evaluate the energy shifts of excitons by only considering the thermal expansion along the in-plane. Figure 4c shows the calculated exciton transition energies as a function of temperature from 4.2 to 300 K. Here, since the coefficients of bilayer WS_2 are not available, the experimentally measured thermal expansion coefficients of bulk WS_2 were used for our calculations.[51] Our results demonstrate that $K-K$ and $K-\Gamma$ transitions have a similar energy shift rate with the decreasing temperature. This indicates that the trend is mainly due to the shift in the K point. In contrast, the trends of $\Lambda-K$ and $\Lambda-\Gamma$ transitions are much slower than $K-K$ and $K-\Gamma$ transitions, suggesting that $K-K$ and $K-\Gamma$ transitions exhibits larger thermal expansion coefficients compared to $\Lambda-K$ and $\Lambda-\Gamma$. The opposite temperature dependence of $\Lambda-K$ and $\Lambda-\Gamma$ found here provides a clue to the origin of the experimentally observed indirect optical transition. Therefore, we can identify that I_1 and I_2 belong to $\Lambda-K$ and $\Lambda-\Gamma$ transitions, respectively. It is obvious that the intensity of I_2 peaks is stronger than I_1 peaks below 80 K, then the intensity of I_1 peak gradually increases and dominates the whole spectra. On the basis of this, it provides a way to engineer the electronic band structures of multilayer WS_2 between the indirect and direct band gap. Similar tunings were also reported in $MoSe_2$ by thermally driving[52] and MoS_2 by hydrostatic pressing.[53]

CONCLUSIONS

In summary, we reported the defect emissions with narrow linewidth, doublet peaks, spatial localization, and saturation behavior in bilayer WS_2. In particular, it can even survive up to 180 K. These characteristics indicate that it may be a good candidate to serve as a single photon source at higher temperatures. By analyzing the temperature-dependent PL spectra of direct and indirect excitons, we obtained the electron−phonon coupling, Debye temperature, temperature and pressure coefficients of the direct and indirect excitons of bilayer WS_2. Combining with the PL experiments and DFT calculations of electronic structures of bilayer WS_2, we identified the origin of the indirect exciton emission and concurrently determined the relative energy of conductance band valleys and valence band hills. Our study provides a better understanding of the energy band structure of bilayer WS_2 and benefits the optoelectronic device designing based on multilayer TMDs.

ASSOCIATED CONTENT

Supporting Information

The Supporting Information is available free of charge on the ACS Publications website at DOI: 10.1021/acs.jpcc.8b11011.

PL spectra of 1-3L WS_2 at room temperature, PL spectra of 3L WS_2 at 4.2 K, defect emission PL spectra of 2L WS_2 at 4.2 K and the details on the fitting parameters (PDF)

AUTHOR INFORMATION

Corresponding Author

*E-mail: zhangjwill@semi.ac.cn.

ORCID

Qing-Hai Tan: 0000-0003-4808-4795
Ping-Heng Tan: 0000-0001-6575-1516
Jun Zhang: 0000-0002-9831-6796

Notes

The authors declare no competing financial interest.

ACKNOWLEDGMENTS

We acknowledge support from the National Basic Research Program of China (grant no. 2017YFA0303401, 2016YFA0301200), NSFC (11574305, 51527901, 11474277, 11434010, and 11225421), and the LU JIAXI International team program supported by the K. C. Wong Education Foundation and the Chinese Academy of Sciences.

REFERENCES

(1) Zhou, Y.; Rasmita, A.; Li, K.; Xiong, Q.; Aharonovich, I.; Gao, W. B. Coherent control of a strongly driven silicon vacancy optical transition in diamond. *Nat. Commun.* **2017**, *8*, 14451.

(2) Leifgen, M.; Schroder, T.; Gadeke, F.; Riemann, R.; Metillon, V.; Neu, E.; Hepp, C.; Arend, C.; Becher, C.; Lauritsen, K.; Benson, O. Evaluation of nitrogen- and silicon-vacancy defect centres as single photon sources in quantum key distribution. *New J. Phys.* **2014**, *16*, 023021.

(3) Benedikter, J.; Kaupp, H.; Hummer, T.; Liang, Y.; Bommer, A.; Becher, C.; Krueger, A.; Smith, J. M.; Hansch, T. W.; Hunger, D. Cavity-Enhanced Single-Photon Source Based on the Silicon-Vacancy Center in Diamond. *Phys. Rev. Appl.* **2017**, *7*, 024031.

(4) Li, K.; Zhou, Y.; Rasmita, A.; Aharonovich, I.; Gao, W. B. Nonblinking Emitters with Nearly Lifetime-Limited Linewidths in CVD Nanodiamonds. *Phys. Rev. Appl.* **2016**, *6*, 024010.

(5) Splendiani, A.; Sun, L.; Zhang, Y.; Li, T.; Kim, J.; Chim, C.-Y.; Galli, G.; Wang, F. Emerging photoluminescence in monolayer MoS_2. *Nano Lett.* **2010**, *10*, 1271−1275.

DOI: 10.1021/acs.jpcc.8b11011
J. Phys. Chem. C 2019, 123, 4433−4440

(6) Mak, K. F.; Lee, C.; Hone, J.; Shan, J.; Heinz, T. F. Atomically Thin MoS_2: A New Direct-Gap Semiconductor. *Phys. Rev. Lett.* **2010**, *105*, 136805.
(7) Chernikov, A.; Berkelbach, T. C.; Hill, H. M.; Rigosi, A.; Li, Y.; Aslan, O. B.; Reichman, D. R.; Hybertsen, M. S.; Heinz, T. F. Exciton Binding Energy and Nonhydrogenic Rydberg Series in Monolayer WS_2. *Phys. Rev. Lett.* **2014**, *113*, 076802.
(8) Cao, T.; Wang, G.; Han, W.; Ye, H.; Zhu, C.; Shi, J.; Niu, Q.; Tan, P.; Wang, E.; Liu, B.; et al. Valley-selective circular dichroism of monolayer molybdenum disulphide. *Nat. Commun.* **2012**, *3*, 887.
(9) Suzuki, R.; Sakano, M.; Zhang, Y.; Akashi, R.; Morikawa, D.; Harasawa, A.; Yaji, K.; Kuroda, K.; Miyamoto, K.; Okuda, T.; et al. Valley-dependent spin polarization in bulk MoS_2 with broken inversion symmetry. *Nat. Nanotechnol.* **2014**, *9*, 611−617.
(10) Srivastava, A.; Sidler, M.; Allain, A. V.; Lembke, D. S.; Kis, A.; Imamoglu, A. Optically active quantum dots in monolayer WSe_2. *Nat. Nanotechnol.* **2015**, *10*, 491−496.
(11) Koperski, M.; Nogajewski, K.; Arora, A.; Cherkez, V.; Mallet, P.; Veuillen, J. Y.; Marcus, J.; Kossacki, P.; Potemski, M. Single photon emitters in exfoliated WSe_2 structures. *Nat. Nanotechnol.* **2015**, *10*, 503−506.
(12) He, Y. M.; Clark, G.; Schaibley, J. R.; He, Y.; Chen, M. -C.; Yu, C. W.; DingXing, J.; Zhang, Q.; Yao, W.; Xu, X.; Lu, C. Y.; Pan, J. W. Single quantum emitters in monolayer semiconductors. *Nat. Nanotechnol.* **2015**, *10*, 497−502.
(13) Chakraborty, C.; Kinnischtzke, L.; Goodfellow, K. M.; Beams, R.; Vamivakas, A. N. Voltage-controlled quantum light from an atomically thin semiconductor. *Nat. Nanotechnol.* **2015**, *10*, 507−511.
(14) Xia, F. N.; Wang, H.; Xiao, D.; Dubey, M.; Ramasubramaniam, A. Two-dimensional material nanophotonics. *Nat. Photonics* **2014**, *8*, 899−907.
(15) Wrachtrup, J. 2D materials: Single photons at room temperature. *Nat. Nanotechnol.* **2016**, *11*, 7−8.
(16) Tonndorf, P.; Schwarz, S.; Kern, J.; Niehues, I.; Pozo-Zamudio, O. D.; Dmitriev, A. I.; Bakhtinov, A. P.; Borisenko, D. N.; Kolesnikov, N. N.; Tartakovskii, A. I.; de Vasconcellos, S. M.; Bratschitsch, R. Single-photon emitters in GaSe. *2D Mater.* **2017**, *4*, 021010.
(17) Tran, T. T.; Bray, K.; Ford, M. J.; Toth, M.; Aharonovich, I. Quantum emission from hexagonal boron nitride monolayers. *Nat. Nanotechnol.* **2016**, *11*, 37−41.
(18) Tran, T. T.; Elbadawi, C.; Totonjian, D.; Lobo, C. J.; Grosso, G.; Moon, H.; Englund, D. R.; Ford, M. J.; Aharonovich, I.; Toth, M. Robust Multicolor Single Photon Emission from Point Defects in Hexagonal Boron Nitride. *ACS Nano* **2016**, *10*, 7331−7338.
(19) Palacios-Berraquero, C.; Matteo, B.; Kara, D. M.; Chen, X.; Ilya, G.; Duhee, Y.; Ott, A. K.; Jan, B.; Kenji, W.; Takashi, T.; et al. Atomically thin quantum light-emitting diodes. *Nat. Commun.* **2016**, *7*, 12978.
(20) Palacios-Berraquero, C.; Kara, D. M.; Montblanch, A. R. P.; Barbone, M.; Latawiec, P.; Yoon, D.; Ott, A. K.; Loncar, M.; Ferrari, A. C.; Atatlżre, M. Large-scale quantum-emitter arrays in atomically thin semiconductors. *Nat. Commun.* **2017**, *8*, 15093.
(21) Kumar, S.; Kaczmarczyk, A.; Gerardot, B. D. Strain-Induced Spatial and Spectral Isolation of Quantum Emitters in Mono- and Bilayer WSe_2. *Nano Lett.* **2015**, *15*, 7567−7573.
(22) Zhao, W. J.; Ribeiro, R. M.; Toh, M.; Carvalho, A.; Kloc, C.; Castro Neto, A. H.; Eda, G. Origin of Indirect Optical Transitions in Few-Layer MoS_2, WS_2, and WSe_2. *Nano Lett.* **2013**, *13*, 5627−5634.
(23) Zhao, W. J.; Ghorannevis, Z.; Chu, L.; Toh, M.; Kloc, C.; Tan, P. H.; Eda, G. Evolution of Electronic Structure in Atomically Thin Sheets of WS_2 and WSe_2. *ACS Nano* **2013**, *7*, 791−797.
(24) Gaur, A. P. S.; Sahoo, S.; Scott, J. F.; Katiyar, R. S. Electron-Phonon Interaction and Double-Resonance Raman Studies in Monolayer WS_2. *J. Phys. Chem. C* **2015**, *119*, 5146−5151.
(25) Zhou, S.; Wang, S.; Li, H.; Xu, W.; Gong, C.; Grossman, J. C.; Warner, J. H. Atomic Structure and Dynamics of Defects in 2D MoS_2 Bilayers. *ACS Omega* **2017**, *2*, 3315−3324.
(26) Li, Y.; Rao, Y.; Mak, K. F.; You, Y.; Wang, S.; Dean, C. R.; Heinz, T. F. Probing Symmetry Properties of Few-Layer MoS_2 and h-BN by Optical Second-Harmonic Generation. *Nano Lett.* **2013**, *13*, 3329−3333.
(27) Tan, P. H.; Han, W. P.; Zhao, W. J.; Wu, Z. H.; Chang, K.; Wang, H.; Wang, Y. F.; Bonini, N.; Marzari, N.; Pugno, N.; Savini, G.; Lombardo, A.; Ferrari, A. C. The shear mode of multilayer graphene. *Nat. Mater.* **2012**, *11*, 294−300.
(28) Zhang, X.; Han, W. P.; Wu, J. B.; Milana, S.; Lu, Y.; Li, Q. Q.; Ferrari, A. C.; Tan, P. H. Raman spectroscopy of shear and layer breathing modes in multilayer MoS_2. *Phys. Rev. B* **2013**, *87*, 115413.
(29) Zhang, X.; Tan, Q. H.; Wu, J. B.; Shi, W.; Tan, P. H. Review on the Raman spectroscopy of different types of layered materials. *Nanoscale* **2016**, *8*, 6435−6450.
(30) Zhao, Y.; Luo, X.; Li, H.; Zhang, J.; Araujo, P. T.; Gan, C. K.; Wu, J.; Zhang, H.; Quek, S. Y.; Dresselhaus, M. S. Interlayer breathing and shear modes in few-trilayer MoS_2 and WSe_2. *Nano Lett.* **2013**, *13*, 1007−1015.
(31) Tan, Q. H.; Sun, Y. J.; Liu, X. L.; Zhao, Y.; Xiong, Q.; Tan, P. H.; Zhang, J. Observation of forbidden phonons, Fano resonance and dark excitons by resonance Raman scattering in few-layer WS_2. *2D Mater.* **2017**, *4*, 031007.
(32) Liang, L.; Zhang, J.; Sumpter, B. G.; Tan, Q. H.; Tan, P. H.; Meunier, V. Low-Frequency Shear and Layer-Breathing Modes in Raman Scattering of Two-Dimensional Materials. *ACS Nano* **2017**, *11*, 11777−11802.
(33) Li, H.; Qing, Z.; Yap, C. C. R.; Beng Kang, T.; Edwin, T. H. J.; Olivier, A.; Baillargeat, D. From Bulk to Monolayer MoS_2: Evolution of Raman Scattering. *Adv. Funct. Mater.* **2012**, *22*, 1385−1390.
(34) Zhang, X.; Qiao, X. F.; Shi, W.; Wu, J. B.; Jiang, D. S.; Tan, P. H. Phonon and Raman scattering of two-dimensional transition metal dichalcogenides from monolayer, multilayer to bulk material. *Chem. Soc. Rev.* **2015**, *44*, 2757−85.
(35) Tan, Q. H.; Zhang, X.; Luo, X. D.; Zhang, J.; Tan, P. H. Layer-number dependent high-frequency vibration modes in few-layer transition metal dichalcogenides induced by interlayer couplings. *J. Semicond.* **2017**, *38*, 031006.
(36) Muller, A.; Flagg, E. B.; Bianucci, P.; Wang, X. Y.; Deppe, D. G.; Ma, W.; Zhang, J.; Salamo, G. J.; Xiao, M.; Shih, C. K. Resonance Fluorescence from a Coherently Driven Semiconductor Quantum Dot in a Cavity. *Phys. Rev. Lett.* **2007**, *99*, 187402.
(37) Flagg, E.; Muller, A.; Robertson, J.; Founta, S.; Deppe, D.; Xiao, M.; Ma, W.; Salamo, G.; Shih, C. K. Resonantly driven coherent oscillations in a solid-state quantum emitter. *Nat. Phys.* **2009**, *5*, 203−207.
(38) Xu, W. G.; Liu, W.; Schmidt, J. F.; Zhao, W.; Lu, X.; Raab, T.; Diederichs, C.; Gao, W.; Seletskiy, D. V.; Xiong, Q. Correlated fluorescence blinking in two-dimensional semiconductor heterostructures. *Nature* **2017**, *541*, 62−67.
(39) Efros, A. L.; Nesbitt, D. J. Origin and control of blinking in quantum dots. *Nat. Nanotechnol.* **2016**, *11*, 661.
(40) Menéndez, J.; Cardona, M. Temperature dependence of the first-order Raman scattering by phonons in Si, Ge, and α-Sn: Anharmonic effects. *Phys. Rev. B* **1984**, *29*, 2051−2059.
(41) Lefevre, G.; Herfurth, A.; Kohlmann, H.; Sayede, A.; Wylezich, T.; Welinski, S.; Duarte Vaz, P.; Parker, S. F.; Blach, J. F.; Goldner, P.; Kunkel, N. Electron-Phonon Coupling in Luminescent Europium-Doped Hydride Perovskites Studied by Luminescence Spectroscopy, Inelastic Neutron Scattering, and First-Principles Calculations. *J. Phys. Chem. C* **2018**, *122*, 10501−10509.
(42) Kentsch, R.; Scholz, M.; Horn, J.; Schlettwein, D.; Oum, K.; Lenzer, T. Exciton Dynamics and Electron-Phonon Coupling Affect the Photovoltaic Performance of the $Cs_2AgBiBr_6$ Double Perovskite. *J. Phys. Chem. C* **2018**, *122*, 25940−25947.
(43) Maddux, C. J. A.; Kelley, D. F.; Kelley, A. M. Weak Exciton-Phonon Coupling in CdSe Nanoplatelets from Quantitative Resonance Raman Intensity Analysis. *J. Phys. Chem. C* **2018**, *122*, 27100−27106.
(44) Monti, M.; Tao, S. X.; Staniforth, M.; Crocker, A.; Griffin, E.; Wijesekara, A.; Hatton, R. A.; Lloyd-Hughes, J. Efficient Intraband Hot Carrier Relaxation in the Perovskite Semiconductor

DOI: 10.1021/acs.jpcc.8b11011
J. Phys. Chem. C 2019, 123, 4433−4440

$Cs_{1-x}Rb_xSnI_3$ Mediated by Strong Electron-Phonon Coupling. *J. Phys. Chem. C* **2018**, *122*, 20669−20675.
(45) Toyozawa, Y. Theory of Line-Shapes of the Exciton Absorption Bands. *Prog. Theor. Phys.* **1958**, *20*, 53−81.
(46) Ho, C.; Wu, C.; Huang, Y.; Liao, P.; Tiong, K. Temperature dependence of energies and broadening parameters of the band-edge excitons of $Mo_{1-x}W_xS_2$ single crystals. *J. Phys.: Condens. Matter* **1998**, *10*, 9317.
(47) Varshni, Y. P. Temperature dependence of energy gap in semiconductors. *Physica* **1967**, *34*, 149.
(48) O'Donnell, K. P.; Chen, X. Temperature dependence of semiconductor band gaps. *Appl. Phys. Lett.* **1991**, *58*, 2924−2926.
(49) Brothers, A. D.; Brungardt, J. B. Excitons in WS_2 films pressure and temperature effects. *Phys. Status Solidi B* **1979**, *91*, 675−679.
(50) Yun, W. S.; Han, S. W.; Hong, S. C.; Kim, I. G.; Lee, J. D. Thickness and strain effects on electronic structures of transition metal dichalcogenides: 2H-MX_2 semiconductors (M = Mo, W; X = S, Se, Te. *Phys. Rev. B* **2012**, *85*, 033305.
(51) Matthaus, A.; Ennaoui, A.; Fiechter, S.; Tiefenbacher, S.; Kiesewetter, T.; Diesner, K.; Sieber, I.; Jaegermann, W.; Tsirlina, T.; Tenne, R. Highly Textured Films of Layered Metal Disulfide 2H-WS_2 and Optoelectronic Properties. *J. Electrochem. Soc.* **1997**, *144*, 1013−1019.
(52) Tongay, S.; Jian, Z.; Ataca, C.; Lo, K.; Matthews, T. S.; Li, J.; Grossman, J. C.; Wu, J. Thermally Driven Crossover from Indirect toward Direct Bandgap in 2D Semiconductors: $MoSe_2$ versus MoS_2. *Nano Lett.* **2012**, *12*, 5576.
(53) Fu, L.; Wan, Y.; Tang, N.; Ding, Y.; Gao, J.; Yu, J.; Guan, H.; Zhang, K.; Wang, W.; Zhang, C.; Shi, J.; Wu, X.; Shi, S.; Ge, W.; Dai, L.; Shen, B. K-Λ crossover transition in the conduction band of monolayer MoS_2 under hydrostatic pressure. *Sci. Adv.* **2017**, *3*, e1700162.

DOI: 10.1021/acs.jpcc.8b11011
J. Phys. Chem. C 2019, 123, 4433−4440